J. Am. Soc. Mass Spectrom. (2012) 23:664–675
DOI: 10.1007/s13361-011-0322-6

FOCUS: MS/MS PEPTIDE IDENTIFICATION: RESEARCH ARTICLE

Rearrangement Pathways of the a_4 Ion of Protonated YGGFL Characterized by IR Spectroscopy and Modeling

Béla Paizs,[1] Benjamin J. Bythell,[1] Philippe Maître[2]

[1]Computational Proteomics Group, German Cancer Research Center (DKFZ), Im Neuenheimer Feld 580, 69120 Heidelberg, Germany
[2]Laboratoire de Chimie Physique, Université Paris Sud, UMR8000 CNRS, Faculté des Sciences, Bât. 350, 91405 Orsay Cedex, France

Abstract

The structure of the a_4 ion from protonated YGGFL was studied in a quadrupole ion trap mass spectrometer by 'action' infrared spectroscopy in the 1000–2000 cm^{-1} ('fingerprint') range using the CLIO Free Electron Laser. The potential energy surface (PES) of this ion was characterized by detailed molecular dynamics scans and density functional theory calculations exploring a large number of isomers and protonation sites. IR and theory indicate the a_4 ion population is primarily populated by the rearranged, linear structure proposed recently (Bythell et al., J. Am. Chem. Soc. 2010, 132, 14766). This structure contains an imine group at the N- terminus and an amide group –CO–NH_2 at the C-terminus. Our data also indicate that the originally proposed N-terminally protonated linear structure and macrocyclic structures (Polfer et al., J. Am. Chem. Soc. 2007, 129, 5887) are also present as minor populations. The clear differences between the present and previous IR spectra are discussed in detail. This mixture of gas-phase structures is also in agreement with the ion mobility spectrum published by Clemmer and co-workers recently (*J. Phys. Chem. A* 2008, *112*, 1286). Additionally, the calculated cross-sections for the rearranged structures indicate these correspond to the most abundant (and previously unassigned) feature in Clemmer's work.

Key words: IR spectroscopy, Modeling, Peptide fragmentation, Sequence ions

Introduction

The formation, structure, and reactivity of b_n and a_n ions (N-terminal fragments [1, 2]) generated in collision-induced dissociation (CID) of protonated peptides have been the subject of detailed studies in the last two decades [3, 4]. The majority of small b_n ions are believed to have a linear backbone terminated by a five-membered oxazolone ring [5–14] at the C-terminus. Exceptions exist if amino acid side chains are involved in the formation of a variety of C-terminal ring structures [15]; typical examples include lysine [16], histidine [17–19], aspartic acid [20], and arginine [21] containing fragments. Formation of fully cyclic isomers of b_n ions has also been proposed [22]. While only a few small b_n fragments form such isomers (for example, protonated-diketopiperazine derivative isomers for b_2 ions) [11–13, 23, 24], the linear, oxazolone-terminated isomers of middle-sized b_n ions can convert to macrocyclic structures by undergoing intramolecular head-to-tail cyclization [25–27].

The formation, structure, and reactivity of a_n ions have received less attention [28]. a_n Ions are formed [5, 6, 29–32] mainly [33] from b_n ions by elimination of CO. According

Electronic supplementary material The online version of this article (doi:10.1007/s13361-011-0322-6) contains supplementary material, which is available to authorized users.

Correspondence to: Béla Paizs; *e-mail:* B.Paizs@dkfz-heidelberg.de, Philippe Maître; *e-mail:* Philippe.Maitre@u-psud.fr

Received: 28 July 2011
Revised: 7 December 2011
Accepted: 13 December 2011
Published online: 24 January 2012

to theory, this reaction proceeds from the linear, oxazolone-terminated b_n ion isomer, initially leading to the linear, protonated imine ($–HN^+=CHR_n$) terminated a_n ion isomer. This type of structure is usually highly reactive and potentially capable of undergoing a variety of reactions. Furthermore, conjugation of the amide bond adjacent to this imine ($–CO–HN^+=CHR_n$) is negligible, thus enabling free rotation around the $CO–HN^+$ axis. For example, this enables linear a_2 ions (formally $H_2N–CHR_1–CO–NH^+=CHR_2$) to undergo head-to-tail cyclization to form a highly stable five-membered ring isomer containing a *cis* amide bond and a secondary amine [28, 34, 35]. In contrast, a_3 ions are rarely detected in the CID spectra of protonated peptides [31, 36], this is ascribed to the characteristic instability of a_3 ions [31]. One of the few observed a_3 ions (GGG sequence) was characterized by IR spectroscopy [28], which showed that a seven-membered ring structure is formed (by nucleophilic attack of the N-terminal amide oxygen on the imine carbon).

Detailed experimental and theoretical data are available for a small number of a_4 and a_5 ions. These ions can also undergo head-to-tail cyclization [9] forming macrocycles with a backbone composed of several amide bonds and a secondary amine. The macrocyclic isomer is energetically as [9], or more [26] stable than the imine protonated linear forms. Importantly, the barrier to cyclization of the protonated imine is only ~10 kcal mol^{-1} [26], allowing facile formation of the macrocycle. An early IR investigation [9] on the a_4 of YGGFL indicated the presence of both linear and macrocyclic forms were likely. Subsequently, an ion mobility spectrometry (IMS) study [37] was performed on the same YGGF a_4 ion. The IM spectrum showed three main features, two of which were assigned to the linear and macrocyclic isomers. The third and most intense IMS peak, corresponding to an intermediate mobility between those of the linear and macrocyclic isomers, remained unassigned [37].

In a very recent combined IR and theoretical study [28] we investigated a larger, expanded selection of potential structures of the a_4 ions of protonated GGGGG and AAAAA. Detailed scans of the corresponding potential energy surfaces indicated the originally formed macrocyclic isomer (with the $–CHR–NH_2^+–CHR'–NH–CO–$ moiety) can undergo proton transfer forming a species protonated at the nitrogen of the amide bond adjacent to the secondary amine ($–CHR–NH–CHR'–NH_2^+–CO–$ moiety). This structure is very labile, specifically with respect to cleavage of the $–CHR'–NH_2^+–$ bond, enabling opening up of the macrocycle to form a rearranged linear isomer terminated by an imine at the N- and an amide group at the C-termini, respectively (i.e., relocating the formerly C-terminal CHR' group at the N-terminal end of the a_4 ion). In the following, we will refer to this rearranged structure as the 'imine-amide' isomer of a_n ions. Our IR studies indicated that the a_4 ion populations of protonated GGGGG and AAAAA are in large part made up of this imine-amide structure under the experimental conditions applied. This is consistent with density functional theory (DFT) calculations, which suggest that the imine-amide structure is energetically substantially more favorable than linear, imine terminated or macrocyclic structures.

In the present paper, we report a follow-up IR and theoretical study of the a_4 ion generated in MS/MS of protonated YGGFL in an ion trap instrument (i.e., just as in a normal proteomics experiment). A very detailed theoretical analysis of the PES is provided, incorporating a far wider variety of potential a_4 ion structures than examined previously [9]. Our new 1000–2000 cm^{-1} spectrum acquired the free electron laser (FEL) at CLIO differs substantially from the previously published spectrum obtained using the FEL at FELIX [9]; potential reasons behind the differences between the two spectra are discussed. Additionally, theoretical collision cross-sections calculated for the structures likely present as indicated by the FELIX and CLIO IR studies are used to help interpret the literature IMS data [37].

Experimental

YGGFL (Sigma Aldrich, Hamburg, Germany) was dissolved in $CH_3OH:H_2O$=1:1 with 2% acetic acid in a concentration range of 50–80 μmol l^{-1} and was sprayed with conventional electrospray (ESI) conditions into a 3D quadrupole ion trap mass spectrometer (Bruker Esquire 3000+; Bremen, Germany). Infrared spectroscopy was carried out using the free electron laser (FEL) at CLIO [38] coupled to the ion trap instrument [39]. Following mass-selection, the isolated $[YGGFL + H]^+$ precursor ions were subjected to CID (MS/MS experiment) to form a_4. Helium was used as the collision gas. The a_4 ions were then mass-selected and irradiated with the FEL IR beam for 200 ms. Our experimental conditions ensure that thermalization of the mass-selected a_4 ions occurs by multiple collisions with helium prior to irradiation with the FEL laser [39]. Upon resonant vibrational excitation, dissociation of a_4 (*m/z* 397.2) was monitored via multiple fragments; a_4^* (*m/z* 380.2), a_4^*-*CO* (*m/z* 352.1), a_4^*-*G* (*m/z* 323.1), a_4^*-*G-CO* (*m/z* 295.2), b_3 (*m/z* 278.1), b_4-*Y* (*m/z* 262.1), a_4-*Y* (*m/z* 234.1), b_2 (*m/z* 221.1), a_2 (*m/z* 193.2), a_4-*Y-G* (*m/z* 177.1), I_Y (*m/z* 136.1), and *m/z* 244.0 and a_2–*CO* (*m/z* 165.0) peaks. The abundances of the a_4 ion and those of the multiple IRMPD fragments listed above were recorded as a function of the IR wavelength in order to derive the IR action spectra where the IRMPD efficiency [40] is plotted against the photon energy.

Computational

A recently developed conformational search engine [3, 7, 9, 11, 21, 23, 24, 26, 27, 41–43] devised to deal with protonated peptides and their fragments was used to scan the potential energy surface (PES) of the a_4 ion of protonated YGGFL. These calculations began with molecular dynamics simulations using the Discover program (Biosym Technologies, San Diego, CA, USA) in conjunction with the AMBER force field [44] modified in-house in order to enable the study of structures

with protonated or neutral imine and oxazolone groups. During the dynamics calculations simulated annealing techniques are used to produce candidate structures for further refinement, applying full geometry optimization using the AMBER force field. These optimized structures were analyzed by a conformer family search program developed in Heidelberg. This program groups optimized structures into families for which the most important characteristic torsion angles of the molecule are similar. The most stable species in the families were then fully optimized at the PM3, HF/3-21G, B3LYP/6-31G(d), and finally at the B3LYP/6-31+G(d,p) levels. The conformer families were regenerated at each level and only structurally nondegenerate conformers were recomputed at the next level to prevent wasting computer time (i.e., only one of N identical structures is recomputed at the next level).

Such series of calculations were performed for the various a_4 isomers (Chart 1) discussed in reference [28] for the a_4 ions of protonated GGGGG and AAAAA. While these calculations adapted L-Tyr for each (A-M) isomers, structures with the Phe residue in both chiral forms were scanned for isomers F, G, H, I, J, K, and L. For species featuring an imine group (A, B, C, D, E, and M) only the *trans* isomerization state was scanned. For the I structures the amide bond adjacent to the secondary amine was considered in the *trans* and *cis* isomerization states. Since head-to-tail cyclization of the parent b_4 ion is possible [25–27] and the observed a_4 photofragments include b_4-*Y* at *m/z* 262.1 (see above) that can be formed from the scrambled GGFY sequence isomer, we scanned the A, B, I, and M a_4 structures with the GGFY sequence as well. All together 29 molecular dynamics scans followed by ab initio and density functional theory calculations were carried out to probe the PES of the a_4 of protonated YGGFL.

The total energies of the various optimized structures are presented in Table S1 (Supplementary Information). Zero-point energy corrected relative energies were computed at the B3LYP/6-31+G(d,p) level. The theoretical IR absorption spectra were determined using harmonic frequencies scaled by a factor of 0.98, as consistently used for IR finger print spectra of b_n [8, 9, 11, 27] and a_n [28] fragments ions at the B3LYP/6-31+G(d,p) level. In order to facilitate the comparison with experimental spectra, the calculated stick spectra were convoluted assuming a Gaussian profile with a 20 cm^{-1} full-width at half-maximum. The same convolution param-

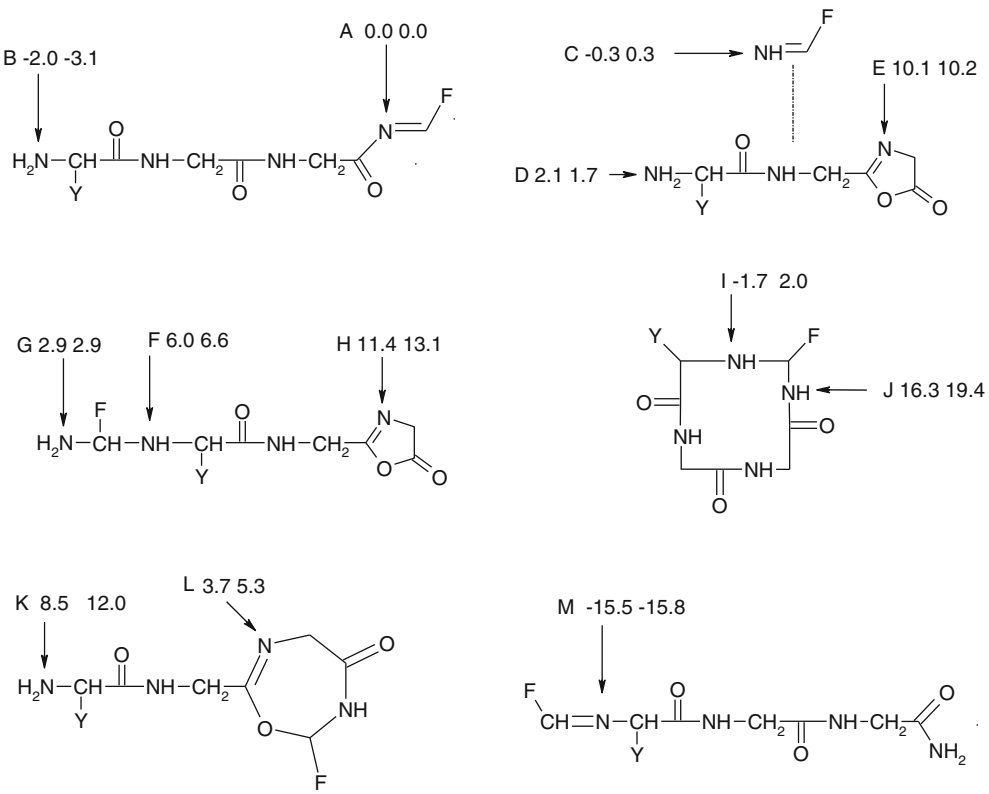

Chart 1. Various structures ($\Delta E_{electronic,0K}$ and ΔG_{298K}) for the a_4 ion of protonated YGGFL: A and B) linear form protonated at the imine nitrogen or N-terminal amino groups, respectively; C, D, and E) proton bound dimers of $NH{=}CH_2$ $-CH_2$-C_6H_5, and 2-(tyrosylaminomethyl)-5-oxazolone protonated at the imine nitrogen, amino group of the oxazolone, or the ring nitrogen of the oxazolone, respectively; F, G, and H) oxazolone terminated re-associated linear form protonated at the secondary amine, N-terminal amino, or ring nitrogen, respectively; I and J) macrocyclic (11-membered ring) isomer protonated at the secondary amine or amide nitrogen, respectively; K and L) seven-membered ring isomer protonated at the N-terminal amine or ring imine nitrogen; and M) rearranged linear form protonated at N-terminal imine group. The respective protonation sites are indicated by arrows. "Y" and "F" denote the side chains of Tyr and Phe, respectively

eters have successfully been used for the analysis of IR fingerprint spectra of other peptide fragments [11, 27, 28]. The Gaussian set of programs [45] was used for all electronic structure, *ab initio* and DFT calculations. Orientation-averaged projection cross sections were obtained for selected structures of the a_4 ions of protonated YGGFL using the Sigma program [46–48] developed by the Bowers group and the Mobcal program developed by the Jarrold group [49] was used to compute collision cross sections based on the trajectory method.

Results and Discussion

The 'fingerprint' (1000–2000 cm^{-1} spectral range) infrared spectrum of the a_4 fragment of protonated YGGFL acquired in the present work is given in Figure 1. For comparison, we also present in Figure 1 the IR spectrum of the same a_4 ion observed [9] previously under experimental conditions significantly differing from those applied in the present work (for more details, see below).

We have recently reported IR spectra for the a_4 ions of protonated GGGGG and AAAAA [28] acquired applying similar experimental conditions (e.g., same mass spectrometer, ion trap CID conditions, IR FEL, etc.). There are similarities and some significant differences between the spectra of the GGGG, AAAA, and YGGF a_4 ions. It is logical that the IR spectra are getting more congested in this series as more complex amino acid side-chains appear. The IRMPD spectrum [28] of the GGGG a_4 ion essentially consists of a single broad band in the 1650 to 1800 cm^{-1} range, with a maximum at 1685 cm^{-1}. The a_4 ion of protonated AAAAA has an additional major band at ~1480 cm^{-1} [28].

In the case of the a_4 ion of protonated YGGFL, the upper frequency (higher wave number) part of our experimental spectrum (Figure 1a) is similar to those obtained for the GGGG and AAAA a_4 ions [28]: a broad band is observed in the amide I region (1680–1750 cm^{-1}) with a shoulder at ~1650 cm^{-1}, and no IRMPD signal was observed above 1800 cm^{-1}. The broad band centered at ~1500 cm^{-1} in the spectrum of the AAAA a_4 ion is also present in the YGGFL spectrum. The main

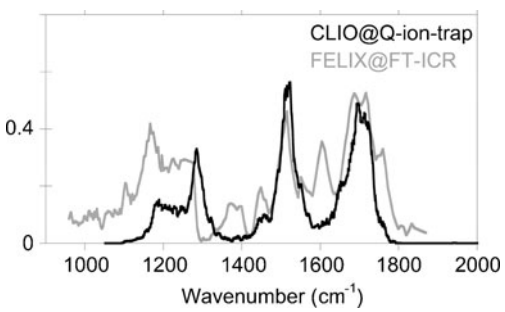

Figure 1. Experimental infrared spectra of the a_4 ions of protonated YGGFL obtained **(a)** in the present work for ions generated via CID within a quadrupole ion trap instrument and (CLIO@Q-ion-trap) **(b)** using SORI-CID within the Penning ion trap of an FT-ICR instrument (FELIX@FT-ICR) [9]

difference between the IRMPD spectrum of the a_4 ion of protonated YGGFL and spectra of the GGGG and AAAA a_4 ions is associated with the lower frequency range. In the YGGFL case, a broad IRMPD band extending from 1150 to 1350 cm^{-1}, with a maximum at ~1280 cm^{-1} is observed, while only a weak (although structured) IRMPD signal could be observed for the GGGG and AAAA a_4 ions.

In our detailed analysis of the IR spectra of the GGGG and AAAA a_4 ions, it was shown that the corresponding ion populations are dominated by the rearranged imine-amide isomer (Structure M in reference [28]). Similarities of the upper frequency part of these IRMPD spectra to that observed for the a_4 of protonated YGGFL suggest that this is likely the case for the latter, too.

Structures and Energetics of the a_4 Ion of Protonated YGGFL

The structural isomers considered for the a_4 ion of protonated YGGFL are shown in Chart 1. The initially formed linear, C-terminal imine protonated isomer (Structure A) also has a second competitive protonation site: the N-terminal amino nitrogen (Structure B). In keeping with our prior study [28], the initially formed imine protonated species (Structure A in Chart 1) will be used as the reference structure here. For the a_4 ion of protonated YGGFL structure B is energetically more favorable than Structure A [9], and can be formed by intramolecular proton transfer.

The reactive imine nitrogen-protonated form of the a_4 ion can undergo a variety of structural transformations (Scheme 1). Nucleophilic attack of the N-terminally adjacent carbonyl oxygen on the C-terminal carbonyl of structure A [50] leads to formation of the five-membered oxazolone ring, cleavage of the CO–NH^+ bond, and expulsion of the Phe-imine (Reaction I, Scheme 1). Under low-energy collision conditions a post-reaction proton-bound dimer (PBD) of HN=CH-CH_2-C_6H_5 and 2-(tyrosyl-glycylaminomethyl)-5-oxazolone is initially formed. Provided this complex is a long-lived enough species under our experimental conditions, which is likely [51], three competitive protonation sites are present: the Phe-imine nitrogen (Structure C in Chart 1) and the N-terminal amino and C-terminal oxazolone-ring nitrogens (Structures D and E in Chart 1, respectively). For the a_4 of protonated YGGFL Structure C is energetically as favorable as Structure A and Structures D and E are energetically less favorable than A.

Attack of the N-terminal amino nitrogen of the oxazolone on the carbon center of the protonated imine enables structure C to undergo a re-association reaction [28, 50, 51] (Reaction Ia, Scheme 1). The isomer formed in this reaction is N-terminated by the H_2N-CH(CH_2-C_6H_5)-NH- group and C-terminated by an oxazolone group. The three competitive protonation sites involve the backbone secondary amine, the N-terminal primary amine, and the oxazolone ring nitrogen, respectively, leading to structures F, G, and H. For the a_4 of protonated YGGFL all these structures are energetically less favored than Structure A (Chart 1).

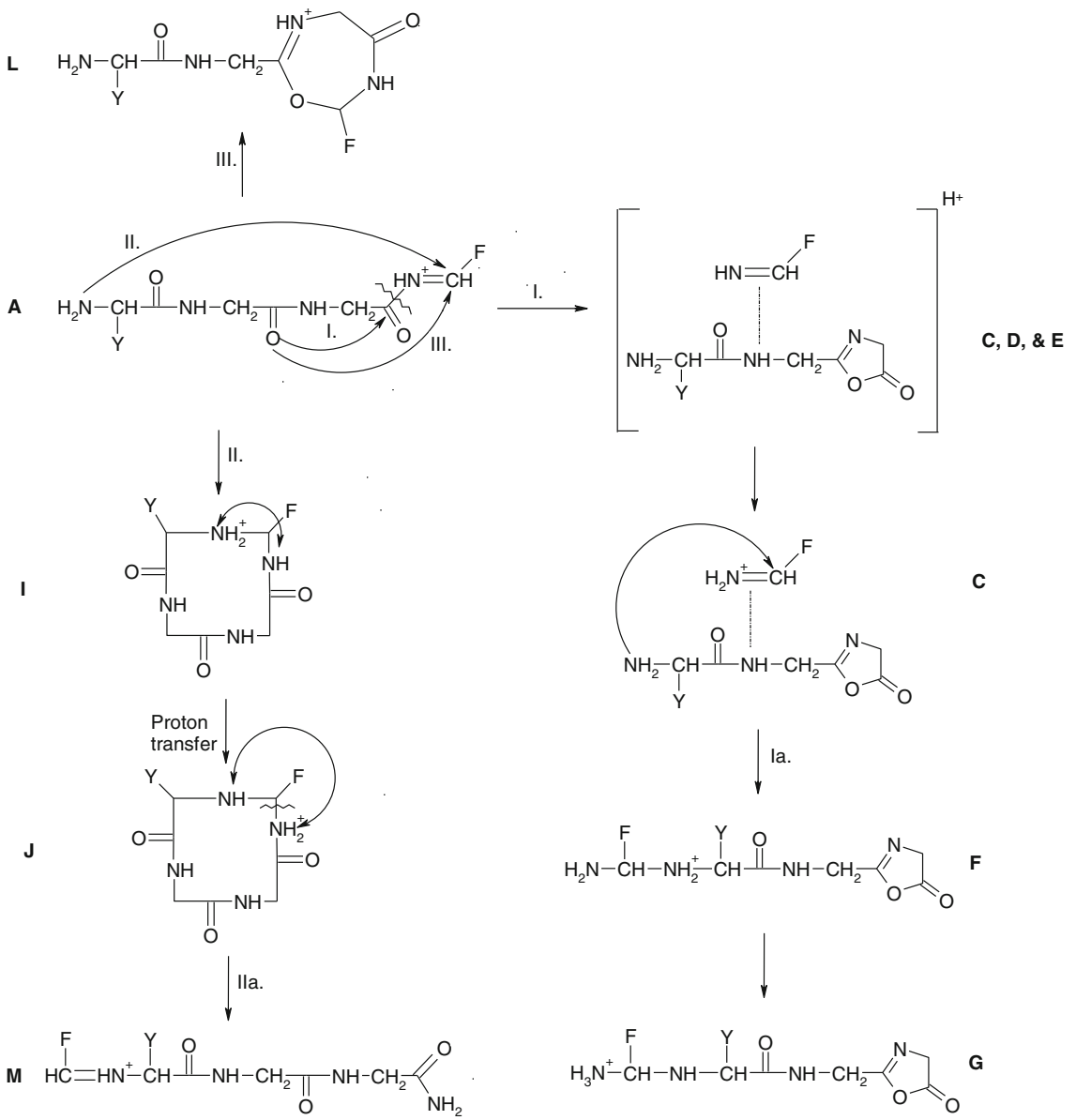

Scheme **1.** Various structures and their reactions for the a_4 ion of protonated YGGFL. Nucleophilic attack (Reaction I) of the carbonyl oxygen of the second residue at the C-terminal carbonyl results in cleavage of the CO-NH^+= bond and formation of the PBD of $NH{=}CH_2$ $–CH_2$-C_6H_5 and 2-(tyrosylaminomethyl)-5-oxazolone (structures C, D, and E). Nucleophilic attack (Reaction Ia) of the N-terminal amino nitrogen of the oxazolone on the carbon center of the protonated imine in C leads to F from which G and H can be formed by intramolecular proton transfer. Nucleophilic attack (Reaction II) of the N-terminal amino nitrogen on the carbon of the protonated imine group can lead to the macrocyclic (11-membered ring) isomer. After proton transfer to the just formed amide bond, leading to Structure J, ring opening occurs forming the rearranged linear Structure M. Nucleophilic attack (Reaction III) of the N-terminal carbonyl oxygen at the C-terminal carbon leads to the 7-membered ring isomer L. "Y" and "F" denote the side chains of Tyr and Phe, respectively

The macrocyclic I isomer of a_4 of protonated YGGFL is formed by nucleophilic attack (Reaction II in Scheme 1) of the N-terminal amino nitrogen on the carbon of the C-terminal protonated imine. Since this reaction can occur 'below' or 'above' the plane of the imine group, formation of two diastereoisomers (L- and D-Phe) was considered in our scans. The macrocycle I is enthalpically slightly more favorable than Structure A, but less so in Gibbs free-energy. Protonation at the nitrogen of the adjacent amide bond (Structure J in Chart 1) [28] has also been probed. The vast majority of the corresponding geometry optimizations led to opening up of the macrocycle to form rearranged imine-amide M structures, leaving only a few meta-stable J structures, the energetically most favorable of these is at 16.3 kcal mol^{-1} relative energy. Our calculations on the rearranged imine-amide M structures indicate that this is the energetically most favorable structure

class on the PES of the a_4 of protonated YGGFL with a relative energy of –15.5 kcal mol^{-1} (Table S1).

Assignment of the IR Spectrum of a_4 of Protonated YGGFL

The IRMPD spectrum of the a_4 ion of protonated YGGFL recorded under our experimental conditions is shown in Figure 2 along with theoretical spectra computed for Structures B, I, and M. As noted above, Structure A is believed to be initially formed via the $b_n \rightarrow a_n$ pathways [30]. However, the IR spectra of the a_4 ions of protonated GGGGG and AAAAA [28] could be assigned by considering either the presence of B, I, and M structures or solely I and M type structures, with the M structure being as the major component of the corresponding a_4 ion populations. Based on this rationale, a band assignment of the IRMPD spectrum of the a_4 of protonated YGGFL is proposed here considering B, I, and M structures in the present section. Theoretical spectra for all other structures presented in Chart 1 were computed (see Figures in the Supplementary Information) and these will be discussed briefly in the subsequent section (these structures have clear spectroscopic signatures that discredit significant population under our experimental conditions).

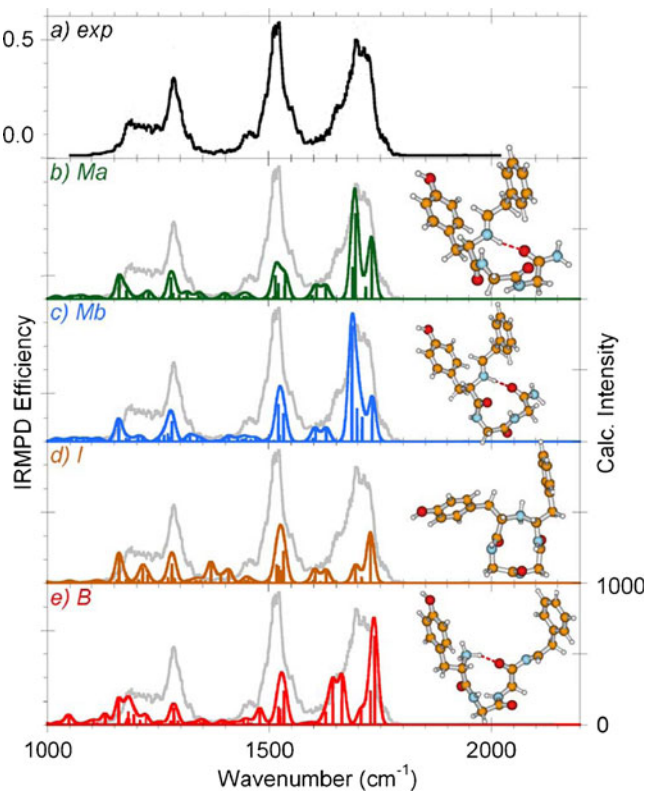

Figure 2. Experimental and calculated infrared spectra of the a_4 ion of protonated YGGFL. Theoretical spectra are presented for two conformers of the rearranged imine-amide form protonated at N-terminal imine (Structures Ma and Mb); the macrocyclic (11-membered ring) isomer protonated at the secondary amine (Structure I); and the N-terminal amino protonated linear form (Structure B)

The assignment of the IR spectra of large, flexible ions featuring a variety of functional groups can be challenging because of a few factors. Molecular ions are thermalized at room temperature through multiple collisions with He within the quadrupole ion trap. It is thus expected that a mixture of multiple conformers of a given isomer may coexist in the ion trap. Unless intramolecular noncovalent interactions vary from one conformer to another, however, the IR absorption spectrum in the fingerprint range of these conformers is not expected to vary significantly. This is illustrated for Structure M in Figure 2, where the calculated IR absorption spectra of two nearly isoenergetic structures (Ma and Mb, Table S1) are given (panels b and c, respectively). As can be seen in Figure 2, the IR absorption spectra predicted for Ma and Mb structures are slightly different in the fingerprint range. While no perfect match is found for the relative intensities of the experimental bands and the theoretical IR intensities computed for each individual structure, one observes that all the IRMPD bands observed experimentally can be explained if one assumes that dissociation occurs when the IR laser is tuned on resonance with IR absorption bands of M type structures.

The two (isoenergetic) M structures considered in Figure 2 have four IR active bands in the ~1640–1780 cm^{-1} range, where the broad experimental band is observed. For example, on the blue side of the experimental band, one finds the amide C=O stretching modes which are predicted at 1716 and 1766 cm^{-1} for structure Ma. The maximum of the broad experimental band at ~1695 cm^{-1} almost coincides with the predicted wave number (1693 cm^{-1}) associated with the C-terminal amide C(NH_2)=O stretching mode, which is predicted to be strongly IR active (600 km/mol). This vibrational mode is nearly degenerate with the C=N stretching mode of the protonated (N-terminal) imine which is predicted at 1688 cm^{-1}. Additionally, the IRMPD band centered at ~1520 cm^{-1} matches with a few closely spaced theoretical modes. For example, amide NH bending modes are predicted to be IR active in this Amide II region (at 1515 and 1535 cm^{-1} for structure Ma). Furthermore, there is also a relatively strongly IR active mode associated with an in-plane CH bending mode of the tyrosine side-chain at about the same wave number (1521 cm^{-1}). The Mb structure gives very similar, but slightly offset values for each band (see Figure 2). For brevity, we do not relist each similar frequency here or in the subsequent text.

The low energy part of the IRMPD spectrum can also be interpreted based on the predicted frequencies of the M structures. A broad experimental band is observed between 1150 and 1350 cm^{-1}. The IRMPD signal is surprisingly constant from 1180 to 1250 cm^{-1}, and then has a maximum at ~1280 cm^{-1}. The two most IR active vibrational modes of structure Ma in this spectral range correspond to two modes of the tyrosine side-chain. These two IR absorption features are shared by all the isomers of the a_4 fragment ion of protonated YGGFL making this range less useful for structural

discrimination. The IRMPD maximum at ~1280 cm^{-1} could be assigned to the tyrosine C–O stretch (1280 cm^{-1}). Conversely, the red-side of the broad band between 1180 and 1250 cm^{-1} could be assigned with the tyrosine COH bending mode which is predicted at 1161 cm^{-1}. At intermediate wavenumbers between these two tyrosine modes, there are several moderately IR active modes (two glycine and one tyrosine CH_2 twisting modes, and in-plane CH bending of the two aromatic rings), which may explain the fact that a nearly constant IRMPD signal is observed in the 1150–1280 cm^{-1} range.

On the basis of the preceding discussion, one might be tempted to conclude that all IRMPD bands can be interpreted solely considering the M structures, rather than considering M as the predominant structure in a mixture composed of a few structures. However, the band observed in the amide I region would be narrower if only M structures were formed. Furthermore, the shoulder (~1650 cm^{-1}) on the red-side of the band at 1680 cm^{-1} cannot be explained if one only considers structure M. It is thus reasonable to assume that other structures of the a_4 ions of protonated YGGFL are formed under our experimental conditions. If one considers a mixture of M structures and, to a minor extent, of B structures formed, one could explain the shape of the broad band observed in the amide I region. Structure B has a strongly IR active C=N stretching mode associated with the imine which is predicted at 1737 cm^{-1} (Figure 2e). More importantly, the shoulder observed at ~1650 cm^{-1} could be the signature of two nearly degenerate modes corresponding to the asymmetric deformation of the protonated N-terminal group ($-N^+H_3$) of Structure B. Additionally, as discussed above, Structure B is more energetically favorable than the initially formed Structure A, making this structure energetically feasible.

Finally, one should also consider the possible formation of macrocyclic structures I. Indeed, in the earlier spectroscopic study of the a_4 ion of protonated YGGFL [9], it was concluded that all experimental bands except 1380 and 1600 cm^{-1} could be interpreted by considering linear, N-terminal amino protonated structures (B in our nomenclature). As can be seen in Figure 2a, no bands could be observed at 1380 and 1600 cm^{-1} in the present case. Although no band could be observed at 1600 cm^{-1}, it should be noticed that the photofragmentation yield is not negligible here. As can be seen in Figure 2d, the lowest energy Structure I has two IR active modes near 1600 cm^{-1}. Structures M, however, also have IR active modes near 1600 cm^{-1}. If these M structures are considered (which was not the case previously [9]), a band near 1600 cm^{-1} cannot be considered as a clear signature of macrocyclic Structure I. A band near 1380 cm^{-1}, as observed in [9], would be a clearer signature of the presence of macrocyclic structure. As can be seen in Figure 2, while structures B and M do not have any significantly IR intense bands between 1300 and 1450 cm^{-1}, the lowest energy Structure I has an IR active mode predicted at 1369 cm^{-1}, which is characteristic to the protonated secondary amine structure since only this isomer type features a NH_2^+ wagging vibration. A zoom-in on the present IRMPD spectrum in the 1380 cm^{-1} region (Figure 2a) shows a very weak IRMPD band near 1380 cm^{-1}. Nevertheless, the signal-to-noise ratio is too low to consider this as proof of significant formation of macrocyclic isomer I under our experimental conditions. To conclude, our IRMPD spectrum is consistent with a mixture of isomers of families M and B, and to some extent a small population of macrocyclic I isomers.

It is worth noting here that our IRMPD experiments do not allow us to draw accurate definitive conclusions on the relative weights of the ion structures composing the overall ion population. This is partly due to the fact that the M, B, and I isomers bear different relative energies and these structures fragment on different pathways. The kinetics of these channels are likely to differ substantially, making quantitative predictions on the relative IRMPD efficiencies of the fragmenting species impractical. Additionally, linear interpretation of band strength with respect to ion population is an area of much debate at present. The consensus is that it is not always a reasonable approach because of our limited understanding of the IRMPD process and its relation to conventional spectroscopy and theoretical calculations used in spectral assignment.

Excluding Other a_4 Ion Structures

Comparison of the IRMPD spectrum with the theoretical IR absorption spectrum of Structure A (the initially formed imine, Figure S1) above ~1580 cm^{-1} enables a clear conclusion; Structure A is not present to any significant extent in our experiment. Structure A is characterized by a protonated C-terminal imine motif which has a characteristic IR active C=O stretching mode predicted at 1831 cm^{-1}. On the other hand, the experimental IRMPD spectrum (Figure 2a) does not have any band above 1800 cm^{-1}. Moreover, the two other amide intense C=O stretching modes are predicted to be at 1648 and 1721 cm^{-1}, where the experimentally recorded IRMPD signal is low. Consequently, one can conclude that the initially formed A-type structures undergo proton transfer and/or rearrangement chemistries leaving no such structures behind.

The calculated IR absorption spectra of Structures C, D, E, F, and G, each of which has a diagnostic oxazolone motif in the 1800–2000 cm^{-1} spectral range, are given in Figure S2. Since no IRMPD signal is observed above 1800 cm^{-1}, it can be safely concluded that these C, D, E, F, and G structures are not present under our experimental conditions. Furthermore, the labile, high energy structure J (16.3 kcal mol^{-1}, Chart 1), is also predicted to have a relatively strongly IR active C=O stretch at 1868 cm^{-1} (Figure S1), which again indicates its absence in the experimental a_4 ion population. Additionally, structures K and L featuring C-terminal seven-membered rings can also be excluded. Structure K has a strong band at 1370 cm^{-1} (Figure S1), which is not observed experimentally, and Structure L has strong bands at 1570 and 1780 cm^{-1} (Figure S1); neither of these is observed experimentally. These structures are energetically disfavored (3.7 and 8.5 kcal mol^{-1}, respectively), so a

negligible or nonexistent population as revealed by IRMPD spectroscopy is in agreement with theory.

YGGF Versus GGFY Sequences

Recent studies [25–27] indicate that middle-sized b_n ions can undergo head-to-tail cyclization by nucleophilic attack of the N-terminal amine on the protonated C-terminal oxazolone ring. While this chemistry becomes facile for b_5 and larger ions, IR spectroscopy [9] of the b_4 ion of protonated YGGFL suggests that at least a small fraction of the b_4 ion population is present as the macrocyclic isomer. Labeling studies support this finding for a_4 and a_5 ions [32]. Ring-opening of this structure can lead in principle to three additional linear oxazolones $GGFY_{oxa}$, $GFYG_{oxa}$, and $FYGG_{oxa}$; the first of these is energetically more favorable than the $YGGF_{oxa}$ [9, 32]. The $GGFY_{oxa}$ b_4 ion can in principle eliminate CO to form $GGFY_{im}$. This chemistry is likely to occur since our a_4 photofragments include b_4-*Y* at *m/z* 262.1 which is a signature of the scrambled GGFY sequence isomer. To gain insight into the related energetics, we performed scans of the corresponding A, B, I, and M a_4 structures with the GGFY sequence (Table S1). The C-terminal imine protonated GGFY isomer is energetically more favored than the corresponding YGGF A structure. On the other hand, the B, I, and M GGFY structures have slightly higher relative energies than the corresponding YGGF species. Altogether no significant differences are observed for the energetics of the YGGF versus GGFY sequence isomers, which were substantially more energetically favorable than the isomers with glycine originally at the C-terminus. Similar conclusions can be drawn about the calculated IR spectra of the GGFY A, B, I, and M structures (Figure S1); these are quite similar to the IR spectra of the corresponding YGGF species. IR spectroscopy in the 'fingerprint' region is a powerful tool to distinguish structural isomers with different functionalities; however it is less effective at compositionally identical, structurally similar species. This is the case for the GGFY versus YGGF isomers in our case.

Comparison of the IR Spectra of a_4 of Protonated YGGFL Recorded at CLIO and FELIX [9]

The infrared spectra of the a_4 ion of protonated YGGFL recorded at FELIX [9] and CLIO (the present work) are clearly different (Figure 1). The differences between these two IR spectra are likely to be due to the fact that different experimental conditions were used for generating and thermalizing the a_4 fragment ions and for irradiating the trapped ion population with the FEL lasers in these experiments. The main structural and energetic characteristics of the CLIO and FELIX FELs are essentially the same and are thus unlikely to cause the observed differences between the two spectra of the a_4 ion of protonated YGGFL. Rather, the method of ion formation and thermalization with the resulting energy (thus population) distribution are likely to be responsible for the observed differences.

The former recorded spectrum [9] was obtained in the Penning trap of a Fourier transform ion cyclotron resonance (FT-ICR) mass spectrometer coupled with the FELIX laser. The a_4 ions were generated within the low pressure Penning ion trap using sustained off-resonance irradiation (SORI-CID) experiments of both the b_4 and protonated YGGFL ions. In the present case, a quadrupole ion trap coupled to the CLIO laser was used, and the a_4 ions were generated within the helium pressurized ion trap using two CID steps: the b_4 ions formed through CID from mass selected protonated YGGFL were subsequently mass-selected to generate a_4 ions. To emphasize the apparent differences in terms of ion formation and thermalization, the acronym CID/QIT/CLIO will be used to refer to our experimental conditions, and SORI/FT-ICR/FELIX will be used to refer to the experimental conditions applied in the previous report [9].

As can be seen in Figure 1, the SORI/FT-ICR/FELIX spectrum has more IRMPD bands than the present CID/QIT/CLIO does. In particular, the main difference between the two experimental spectra is the presence of two bands at 1380 and 1600 cm^{-1} in the SORI/FT-ICR/FELIX experimental spectrum. In the CID/QIT/CLIO case, however, no strong band is observed at 1380 cm^{-1}, and while an IRMPD signal is observed at 1600 cm^{-1}, no maximum was present at this wave number. In this section, we discuss possible origins for these spectral differences.

Analysis of the SORI/FT-ICR/FELIX spectrum and theoretical spectra for a limited set of structures of the a_4 ion of protonated YGGFL [9] led to the conclusion that a mixture of two isomers was formed. All experimental bands except 1380 and 1600 cm^{-1} were interpreted by considering linear, N-terminal amino protonated structures (B in our nomenclature). Consequently, it was concluded that the linear form B predominated the a_4 ion population generated by SORI-CID in the FT-ICR. Comparison of the FELIX IRMPD spectrum with the calculated absorption spectrum of a macrocyclic isomer (structure family I in the present paper but *not* the same structure presented in Figure 2) suggested that the two experimental features at 1380 and 1600 cm^{-1} could be signatures of this macrocyclic isomer. This I structure has two IR active modes associated with the $-NH_2^+-$ group corresponding to the wagging and the scissoring modes, which are predicted at 1369 and 1604 cm^{-1}, respectively. Furthermore, all other calculated IR absorption features of the macrocyclic structure were compatible with the observed photodissociation spectrum of the a_4 ion. Therefore, it was reasonable to assume that the linear B and macrocyclic I structures were the only components of the a_4 ion population.

It is important to note here that the rearranged M isomer was not considered in the analysis of the FELIX spectrum [9] since this structure had not been thought of at that time. In the present work, no clear experimental features can be observed at 1380 and 1600 cm^{-1}. As a result, the formation

of a large amount of I-type structures cannot be envisaged. This led us to reinvestigate the potential energy surface of the a_4 ions, and a larger set of structures was tested against our new CID/QIT/CLIO IRMPD spectrum. Our detailed analysis indicates that structures of the imine-amide (M) family are predominantly present under the experimental conditions applied while Structure B represents a much less abundant component.

The experimental conditions under which the CID/QIT/CLIO IRMPD and SORI/FT-ICR/FELIX spectra were obtained differ substantially, with the main difference being associated with the ion formation process and subsequent thermalization. Our experiments were performed in a quadrupole ion trap with helium pressure of ~10^{-3} mbar. The a_4 fragment ions were formed in the MS/MS stage by fragmentation of protonated YGGFL (i.e., in the same manner as is normally implemented in usual peptide sequencing experiments). The a_4 ions were then mass-selected and subsequently fragmented using the FEL IR beam. Furthermore, due to the relatively high helium pressure within the quadrupole ion trap, mass-selected a_4 fragment ions are likely to be thermalized at room temperature prior to their irradiation.

Conversely, in the SORI/FT-ICR/FELIX experiment [9], the CID process was performed in an ICR cell using SORI-CID at comparatively low pressure (2×10^{-7} mbar). SORI-CID was simultaneously performed on protonated YGGFL and its b_4 fragment to generate the a_4 ion population. That is, a_4 ions were not all formed in the usual, single stage MS/MS experiment that is routinely applied for peptide sequencing in proteomics. Furthermore, the relative low pressure of collision gas in the Penning ion trap is likely to be less effective at enabling fast thermalization of the a_4 ions prior to their irradiation with the FELIX IR beam.

The FELIX and CLIO free electron lasers have very similar characteristics. In particular, their temporal structures are the same, except that the macropulse repetition rate is higher at CLIO (25 Hz) than at FELIX (10 Hz). It is worth noting here that the irradiation time for the present experiment was only 200 ms (i.e., 5 macropulses at 25 Hz), whereas much longer irradiation time of 4 s (40 macropulses at 10 Hz) was used at FELIX [9]. Despite this longer irradiation time, only the a_4^* (*m/z* 380.2) and b_3 (*m/z* 278.1) photofragments were observed in the latter [9]. In contrast, more pronounced (sequential) fragmentation was achieved in the present case since multiple fragments [a_4^* (*m/z* 380.2), a_4^*-*CO* (*m/z* 352.1), a_4^*-*G* (*m/z* 323.1), a_4^*-*G-CO* (*m/z* 295.2), b_3 (*m/z* 278.1), b_4-*Y* (*m/z* 262.1), a_4-*Y* (*m/z* 234.1), b_2 (*m/z* 221.1), a_2 (*m/z* 193.2), a_4-*Y-G* (*m/z* 177.1), I_Y (*m/z* 136.1), and *m/z* 244.0 and a_2–*CO* (*m/z* 165.0)] were observed. This is consistent with previous observations, where a large [52] or even total depletion [39] of the parent ion population could be observed using a single FEL macropulse (~8 μs at 25 Hz at CLIO) when the parent ions are confined in a quadrupole ion trap. As discussed previously [39], this is likely to be due to the much better ion confinement with the quadrupole ion trap than in the ICR trap. It should also be noted that when the laser beam is parallel to the magnetic field, shorter irradiation time period can be used [53] than when the IR beam is perpendicular to the magnetic field, as in the configuration of the FT-ICR at FELIX.

To summarize, the experimental conditions used to acquire the CID/IT/CLIO spectrum in this work are such that fragment ions are thermalized prior to the irradiation. In contrast, the low pressure of the SORI collision gas within the ICR cell used for the SORI/FT-ICR/FELIX experiment hampers efficient thermalization of the ions; this is likely to be a source of broadening of the IRMPD bands. It should also be noted that another source of difference between the two experimental spectra is that the SORI/FT-ICR/FELIX spectrum was presented as a depletion of the parent signal. In our case, the experimental IRMPD spectrum is the photodissociation yield as a function of the wavelength. As clearly shown in a recent paper [54], this could also be a contributing factor to the bands reported previously [9] being broader than in the present study. As found in the case of other peptide fragment ions, it seems that when CID is performed within the quadrupole ion trap, the kinetically most favored isomer is predominantly formed provided sufficient energy is available to enable its formation. In the SORI/FT-ICR/FELIX experiment, however, more structures are explored, opening up ways to assess species not detectable in the CID/QIT/CLIO case. Both experimental setups seem to have their own strengths and limitations, and we encourage the ion spectroscopy community to investigate these characteristics in further detail.

Comparison of Experimental [37] and Theoretical Collision Cross-Sections for the a_4 Ion of Protonated YGGFL

The preceding discussion on the IR spectra led to the conclusion that the M, B, and I isomers should be considered

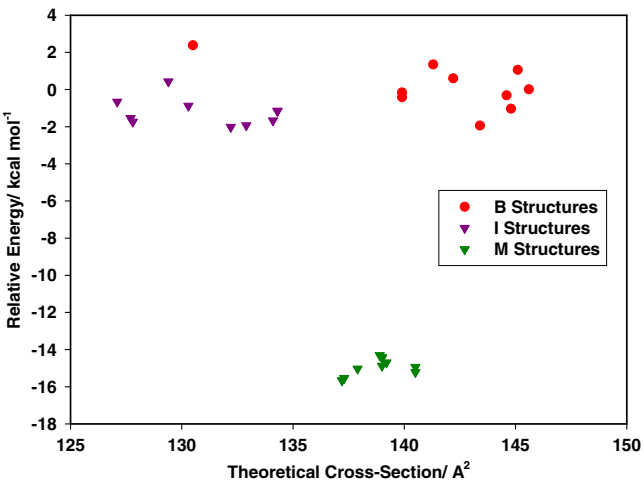

Figure 3. Relative energies (kcal mol^{-1}) versus calculated collision cross sections (Å^2, TM method) plotted for the energetically most favorable B, I, and M structures of the a_4 ion of protonated YGGFL

as the most likely populated isomers of the a_4 ion of protonated YGGFL under ion trapping conditions. It should be stressed, however, that the relative abundances of these isomers strongly depend on experimental conditions used for generating and fragmenting the precursor ions, and also for thermalizing the fragment ions. A mixture of three isomers is consistent with the ion mobility data in the literature for the same a_4 ion [37]. The experimentally determined collision cross-section distribution showed two overlapping peaks at 127–131 and 133–137 Å^2, corresponding to 31% and 61% relative abundances, and a third peak at 143–146 Å^2 corresponding to a weaker (8%) abundance. In the original IMS paper [37], the two peaks corresponding to the smallest and largest collision cross-sections were assigned to the macrocyclic (Structure I) and the amino protonated linear imine (Structure B) structures, respectively. At that time, the most abundant feature in the 133–137 Å^2 range could not be unambiguously assigned. From the present IR spectroscopic and theoretical data however, one can see that the rearranged imine-amide M structure is a reasonable candidate for interpreting the unassigned peak in the ion mobility spectrum.

To probe this hypothesis we determined theoretical collision cross-sections (Figure 3) for the most stable B, I, and M structures of a_4 of protonated YGGFL. To compute these we adopted the orientation-averaged projection approximation (PA) as implemented in the Sigma program [46–48] developed in the Bowers group and the trajectory method (TM) [49] as implemented in the Mobcal program developed by the Jarrold group. The PA method predicts smaller theoretical cross-sections than those obtained by TM. As the TM method was used in the original IMS work on the a_4 of protonated YGGFL [37], for brevity only the TM results will be discussed here.

As expected, the macrocyclic I structures are characterized by the lowest computed collision cross-sections (10 lowest-energy structures in the 127–134 Å^2 range, 131.0 Å^2 average value computed without considering weighting with relative energy). These macrocyclic structures are likely to account for the experimental IMS feature with the highest mobility. The cross-sections for the M structures spread a relatively narrow range (137–140 Å^2, 138.9 Å^2 average value computed without considering weighting with relative energy). The presence of the M structures is thus consistent with the experimental IMS feature for the 133–137 Å^2 range. It is worth noting here that the M imine-amide isomer is energetically much more favorable than the other isomers. The calculated cross-sections for the B isomers (140–146 Å^2, with a single outliner at 130.5 Å^2 (the highest-energy structure from the considered 10, 142.9 Å^2 average value computed for the energetically most favored nine structures without considering weighting with relative energy) are consistent with the experimental values (143–145 Å^2) obtained for the feature representing the species with the least mobility. Therefore, the main experimental IMS features [37] are reasonably explained based on the theoretical structures presented in this work by assuming that B, I, and also M structures are populated in the IMS instrument.

Conclusions

Our combined IRMPD and theoretical analysis indicates the ion population of the a_4 ion of protonated YGGFL in our ion trap is predominantly composed of M-type imine-amide structures. Linear, N-terminal amine protonated species (Structure B) and to a lesser extent macrocyclic forms (Structure I) are also possibly present. This indicates that the imine-amide isomers previously described only for the a_4 ions with the GGGG and AAAA sequences are likely to be present more generally. The new IRMPD spectrum of the a_4 ion of protonated YGGFL obtained here differs significantly from the literature spectrum of the same ion acquired under significantly different experimental conditions in terms of ion formation, thermalization after formation and, to a lesser extent, interaction of the ion cloud with the FEL laser. These differences were described and discussed in detail, and the gas-phase ion chemistry community is urged to implement further studies to enable a better understanding of this phenomenon. Collision cross-section calculations indicate that the simultaneous presence of M, B, and I type structures in the mass spectrometer is consistent with earlier ion mobility data for the same a_4 ion explaining the tri-modal IMS spectrum features and the so far unassigned IMS peak.

Acknowledgements

B.P. thanks the Deutsche Forschungsgemeinschaft for a Heisenberg fellowship. B.B. thanks the DKFZ for a guest scientist fellowship. Financial support by the European Commission (seventh framework programme, grant number 226716) is gratefully acknowledged. The authors are grateful to J. M. Ortega, J. P. Berthet, J. Lemaire, and V. Steinmetz for technical support. They thank Jos Oomens for useful discussions.

References

1. Roepstorff, P., Fohlmann, J.: Proposals for a common nomenclature for sequence ions in mass spectra of peptides. *Biomed. Mass Spectrom.* **11**, 601 (1984)
2. Biemann, K.: Contributions of mass spectrometry to peptide and protein structure. *Biomed. Environ. Mass Spectrom.* **16**, 99–111 (1988)
3. Paizs, B., Suhai, S.: Fragmentation pathways of protonated peptides. *Mass Spectrom. Rev.* **24**, 508–548 (2005)
4. Harrison, A.G.: To b or not to b: The ongoing saga of peptide b ions. *Mass Spectrom. Rev.* **28**, 640–654 (2009)
5. Yalcin, T., Khouw, C., Csizmadia, I.G., Peterson, M.R., Harrison, A.G.: Why are B ions stable species in peptide mass spectra? *J. Am. Soc. Mass Spectrom.* **6**, 1165–1174 (1995)
6. Yalcin, T., Csizmadia, I.G., Peterson, M.R., Harrison, A.G.: The structures and fragmentation of B_n ($n \geq 3$) ions in peptide mass spectra. *J. Am. Soc. Mass Spectrom.* **7**, 233–242 (1996)
7. Paizs, B., Lendvay, G., Vékey, K., Suhai, S.: Formation of b_2^+ ions from protonated peptides: An ab initio study. *Rapid Commun. Mass Spectrom.* **13**, 525–533 (1999)
8. Polfer, N.C., Oomens, J., Suhai, S., Paizs, B.: Spectroscopic and theoretical evidence for oxazolone ring formation in collision-induced dissociation of peptides. *J. Am. Chem. Soc.* **127**, 17154–17155 (2005)

9. Polfer, N.C., Oomens, J., Suhai, S., Paizs, B.: Infrared spectroscopy and theoretical studies on gas-phase protonated leu-enkephalin and its fragments: Direct experimental evidence for the mobile proton. *J. Am. Chem. Soc.* **129**, 5887–5897 (2007)
10. Yoon, S.H., Chamot-Rooke, J., Perkins, B.R., Hilderbrand, A.E., Poutsma, J.C., Wysocki, V.H.: IRMPD spectroscopy shows that AGG forms an oxazolone b_2^+ ion. *J. Am. Chem. Soc.* **130**, 17644–17645 (2008)
11. Bythell, B.J., Erlekam, U., Paizs, B., Maitre, P.: Infrared spectroscopy of fragments derived from tryptic peptides. *ChemPhysChem* **10**, 883–885 (2009)
12. Bythell, B.J., Somogyi, Á., Paizs, B.: What is the structure of b_2 ions generated from doubly protonated tryptic peptides? *J. Am. Soc. Mass Spectrom.* **20**, 618–624 (2009)
13. Chen, X., Turecek, F.: Simple b-ions have cyclic structures. A neutralization-reionization mass spectrometric and computational study. *J. Am. Soc. Mass Spectrom.* **16**, *1941–1956 (2005)*
14. Sinha, R.K., Erlekam, U., Bythell, B.J., Paizs, B., Maître, P.: Diagnosing the protonation site of b_2 peptide fragment ions using IRMPD in the X–H (X=O, N, and C) stretching region. *J. Am. Soc. Mass Spectrom.* **22**, 1645–1650 (2011)
15. Farrugia, J.M., O'Hair, R.A.J., Reid, G.A.: Do all b_2 ions have oxazolone structures? Multistage mass spectrometry and ab initio studies on protonated N-acyl amino acid methyl ester model systems. *Int. J. Mass Spectrom.* **210–211**, 71–87 (2001)
16. Yalcin, T., Harrison, A.G.: Ion chemistry of protonated lysine derivatives. *J. Mass Spectrom.* **31**, 1237–1243 (1996)
17. Farrugia, J.M., Taverner, T., O'Hair, R.A.J.: Side-chain involvement in the fragmentation reactions of protonated methyl esters of histidine and its peptides. *Int. J. Mass Spectrom.* **209**, 99–112 (2001)
18. Knapp-Mohammady, M., Young, A.B., Paizs, B., Harrison, A.G.: Fragmentation of doubly-protonated Pro-His-Xaa tripeptides: Formation of b_2^{2+} ions. *J. Am. Soc. Mass Spectrom.* **20**, 2135–2143 (2009)
19. Tsaprailis, G., Nair, H., Zhong, W., Kuppannan, K., Futrell, J.H., Wysocki, V.H.: A mechanistic investigation of the enhanced cleavage at histidine in the gas-phase dissociation of protonated peptides. *Anal. Chem.* **76**, 2083–2094 (2004)
20. Yu, W., Vath, J.E., Huberty, M.C., Martin, S.A.: Identification of the facile gas-phase cleavage of the Asp-Pro and Asp-Xxx peptide bonds in matrix assisted laser desorption time-of-flight mass spectrometry. *Anal. Chem.* **65**, 3015–3023 (1993)
21. Bythell, B.J., Csonka, I.P., Suhai, S., Barofsky, D.F., Paizs, B.: Gas-phase structure and fragmentation pathways of singly protonated peptides with N-terminal arginine. *J. Phys. Chem. B* **114**, 15092–15105 (2010)
22. Cordero, M.M., Houser, J.J., Wesdemiotis, C.: The neutral products formed during backbone fragmentations of protonated peptides in tandem mass spectrometry. *Anal. Chem.* **65**, 1594–1601 (1993)
23. Paizs, B., Suhai, S.: Combined quantum chemical and RRKM modeling of the main fragmentation pathways of protonated GGG. II. Formation of b_2, y_1, and y_2 ions. *Rapid Commun. Mass Spectrom.* **16**, 375–389 (2002)
24. Paizs, B., Suhai, S.: Towards understanding the tandem mass spectra of protonated oligopeptides. 1: Mechanism of amide bond cleavage. *J. Am. Soc. Mass Spectrom.* **15**, 103–113 (2004)
25. Harrison, A.G., Young, A.B., Bleiholder, C., Suhai, S., Paizs, B.: Scrambling of sequence information in collision-induced dissociation of peptides. *J. Am. Chem. Soc.* **128**, 10364–10365 (2006)
26. Bleiholder, C., Osburn, S., Williams, T.D., Suhai, S., Van Stipdonk, M., Harrison, A.G., Paizs, B.: Sequence-scrambling pathways of protonated peptides. *J. Am. Chem. Soc.* **130**, 17774–17789 (2008)
27. Erlekam, U., Bythell, B.J., Scuderi, D., Van Stipdonk, M., Paizs, B., Maitre, P.: Infrared spectroscopy of fragments of protonated peptides. Direct evidence for macrocyclic structure of b_5 ions. *J. Am. Chem. Soc.* **131**, 11503–11508 (2009)
28. Bythell, B.J., Maître, P., Paizs, B.: Cyclization and rearrangement reactions of a_n fragment ions of protonated peptides. *J. Am. Chem. Soc.* **132**, 14766–14779 (2010)
29. Ambihapathy, K., Yalcin, T., Leung, H.-W., Harrison, A.G.: Pathways to immonium ions in the fragmentation of protonated peptides. *J. Mass Spectrom.* **32**, 209–215 (1997)
30. Paizs, B., Szlavik, Z., Lendvay, G., Vekey, K., Suhai, S.: Formation of a_2^+ ions of protonated peptides. An ab initio study. *Rapid Commun. Mass Spectrom.* **14**, 746–755 (2000)
31. Allen, J.M., Racine, A.H., Berman, A.M., Johnson, J.S., Bythell, B.J., Paizs, B., Glish, G.L.: Why are a_3 ions rarely observed? *J. Am. Soc. Mass Spectrom.* **19**, 1764–1770 (2008)
32. Bythell, B.J., Molesworth, S., Osburn, S., Cooper, T., Paizs, B., Van Stipdonk, M.: Structure and reactivity of a_n and a_n* peptide fragments investigated using isotope labeling, tandem mass spectrometry, and density functional theory calculations. *J. Am. Soc. Mass Spectrom.* **19**, 1788–1798 (2008)
33. Vachet, R.W., Ray, K.L., Glish, G.L.: Origin of product ions in the MS/MS spectra of peptides in a quadrupole ion trap. *J. Am. Soc. Mass Spectrom.* **9**, 341–344 (1998)
34. El Aribi, H., Rodriquez, C.F., Almeida, D.R.P., Ling, Y., Mak, W.N.V., Hopkinson, A.C., Siu, K.W.M.: Elucidation of fragmentation mechanisms of protonated peptide ions and their products: A case study on Glycylglycylglycine using density functional theory and threshold collision-induced dissociation. *J. Am. Chem. Soc.* **125**, 9229–9236 (2003)
35. Verkerk, U.H., Siu, C.-K., Steill, J.D., El Aribi, H., Zhao, J., Rodriquez, C.F., Oomens, J., Hopkinson, A.C., Michael Siu, K.W.M.: a_2 ion derived from triglycine: An N_1-protonated 4-imidazolidinone. *J. Phys. Chem. Lett.* **1**, 868–872 (2010)
36. Savitski, M.M., Falth, M., Eva Fung, Y.M., Adams, C.M., Zubarev, R. A.: Bifurcating fragmentation behavior of gas-phase tryptic peptide dications in collisional activation. *J. Am. Soc. Mass Spectrom.* **19**, 1755–1763 (2008)
37. Polfer, N.C., Bohrer, B.C., Plasencia, M.D., Paizs, B., Clemmer, D.E.: On the dynamics of fragment isomerization in collision-induced dissociation of peptides. *J. Phys. Chem. A* **112**, 1286–1293 (2008)
38. Prazeres, R., Glotin, F., Insa, C., Jaroszynski, D.A., Ortega, J.M.: Two-color operation of a free-electron laser and applications in the mid-infrared. *Eur. Phys. J. D* **3**, 87–93 (1998)
39. MacAleese, L., Simon, A., McMahon, T.B., Ortega, J.M., Scuderi, D., Lemaire, J., Maître, P.: Mid-IR spectroscopy of protonated leucine methyl ester performed with an FTICR or a Paul type ion-trap. *Int. J. Mass. Spectrom.* **249/250**, 14–20 (2006)
40. Lemaire, J., Boissel, P., Heninger, M., Mauclaire, G., Bellec, G., Mestdagh, H., Simon, A., Caer, S.L., Ortega, J.M., Glotin, F., Maitre, P.: Gas phase infrared spectroscopy of selectively prepared ions. *Phys. Rev. Lett.* **89**, 273002–273004 (2002)
41. Bythell, B.J., Suhai, S., Somogyi, A., Paizs, B.: Proton-driven amide bond-cleavage pathways of gas-phase peptide ions lacking mobile protons. *J. Am. Chem. Soc.* **131**, 14057–14065 (2009)
42. Wyttenbach, T., Paizs, B., Barran, P., Breci, L., Liu, D., Suhai, S., Wysocki, V.H., Bowers, M.: The effect of the initial water of hydration on the energetics, structures, and H/D exchange mechanism of a family of pentapeptides: An experimental and theoretical study. *J. Am. Chem. Soc.* **125**, 13768–13775 (2003)
43. Paizs, B., Suhai, S., Hargittai, B., Hruby, V.J., Somogyi, A.: Ab initio and MS/MS studies on protonated peptides containing basic and acidic amino acid residues. I. Solvated proton vs. salt-bridged structures and the cleavage of the terminal amide bond of protonated RD-NH_2. *Int. J. Mass Spectrom.* **219**, 203–232 (2002)
44. Case, D.A., Pearlman, D.A., Caldwell, J.W., Cheatham III, T.E., Ross, W. S., Simmerling, C.L., Darden, T.A., Merz, K.M., Stanton, R.V., Cheng, A. L., Vincent, J.J., Crowley, M., Tsui, V., Radmer, R.J., Duan, Y., Pitera, J., Massova, I.G., Seibel, G.L., Singh, U.C., Weiner, P.K., Kollmann, P.A.: In: AMBER 99, University of California, San Francisco (1999)
45. Frisch, M.J., et al.: Gaussian 03. Gaussian Inc., Pittsburgh (2003)
46. von Helden, G., Hsu, M.-T., Gotts, N., Bowers, M.T.: Carbon cluster cations with up to 84 atoms: Structures, formation mechanism, and reactivity. *J. Phys. Chem.* **97**, 8182–8192 (1993)
47. Wyttenbach, T., von Helden, G., Batka, J.J., Carlat, D., Bowers, M.T.: Effect of the long-range potential on ion mobility measurements. *J. Am. Soc. Mass Spectrom.* **8**, 275–282 (1997)
48. Wyttenbach, T., Witt, M., Bowers, M.T.: On the stability of amino acid zwitterions in the gas phase: The influence of derivatization, proton affinity, and alkali ion addition. *J. Am. Chem. Soc.* **122**, 3458–3464 (2000)
49. Mesleh, M.F., Hunter, J.M., Shvartsburg, A.A., Schatz, G.C., Jarrold, M.F.: Structural information from ion mobility measurements: Effects of the long range potential. *J. Phys. Chem.* **100**, 16082–16086 (1996)
50. Cooper, T., Talaty, E., Grove, J., Suhai, S., Paizs, B., Van Stipdonk, M.: Isotope labeling and theoretical study of the formation of a_3* ions from protonated tetraglycine. *J. Am. Soc. Mass Spectrom.* **17**, 1654–1664 (2006)

51. Bythell, B.J., Barofsky, D.F., Pingitore, F., Wang, P., Wesdemiotis, C., Paizs, B.: Backbone cleavages and sequential loss of carbon monoxide and ammonia from protonated AGG: A combined tandem mass spectrometry, isotope labeling, and theoretical study. *J. Am. Soc. Mass Spectrom.* **18**, 1291–1303 (2007)
52. Salpin, J.Y., Guillaumont, S., Tortajada, J., MacAleese, L., Lemaire, J., Maitre, P.: Infrared spectra of protonated uracil, thymine and cytosine. *ChemPhysChem* **8**, 2235–2244 (2007)
53. Bakker, J.M., Besson, T., Lemaire, J., Scuderi, D., Maitre, P.: Gas-phase structure of a -allyl-palladium complex: Efficient infrared spectroscopy in a 7T fourier transform mass spectrometer. *J. Phys. Chem. A* **111**, 13415–13424 (2007)
54. Prell, J.S., O'Brien, J.T., Williams, E.R.: IRPD spectroscopy and ensemble measurements: Effects of different data acquisition and analysis methods. *J. Am. Soc. Mass Spectrom.* **21**, 800–809 (2010)